JOURNAL OF GEOPHYSICAL RESEARCH, VOL. 90, NO. A3, PAGES 2792–2806, MARCH 1, 1985

High-Amplitude VLF Transmitter Signals and Associated Sidebands Observed Near the Magnetic Equatorial Plane on the ISEE 1 Satellite

T. F. BELL

STAR Lab, Stanford University, California

On February 16, 1983, during a period of strong magnetic disturbance ($K_p \sim 5$), as the ISEE 1 satellite passed near the magnetic meridian of the Omega navigation transmitter (98°W, 46°N geographic, $L \sim 3.4$), the Stanford University VLF wave receiver detected the presence of Omega transmitter signals over the range $2 \leq L \leq 3.7$ at magnetic latitudes (λ_m) within 10° of the magnetic equator. Over a 500-km orbital segment near $L \sim 3.4$ and $\lambda_m \sim 5°$S, the electric field amplitude of the Omega signals reached ~ 0.6 mV/m, a value > 40dB higher than the signal amplitude both preceding ($L \sim 3.7 - 3.5$) and following ($L \leq 3.2$) the high-amplitude period. Over the range $3.3 \leq L \leq 3.7$ the transmitter pulses at 13.1 and 13.6 kHz were associated with sideband signals spaced in frequency roughly symmetrically about the carrier and generally reduced in amplitude ~5 dB with respect to the carrier. The strongest sidebands were generally offset in frequency from the carrier by $\sim \pm 55$ Hz. Simultaneous data from the University of Iowa Plasma Wave experiment indicated that the region of high wave amplitude was located just beyond the outer edge of the plasmapause where low values of cold plasma density (~ 40 el/cm^3) prevailed. High amplitudes were observed only during the time in which the signal frequency lay within the range of a natural noise band of rising center frequency in which bursts of VLF emissions were occasionally triggered by "knee-trace" whistlers. On the basis of the group time delay and amplitude distribution of the Omega signals and the presence of knee-trace whistlers, it is concluded that the high amplitude signals originally propagated along the base of the plasmapause surface into the southern hemisphere and subsequently reflected or scattered back up to the satellite. The high-wave amplitude was presumably produced through the coherent whistler mode instability as the input waves interacted with gyroresonant energetic electrons near the magnetic equatorial plane, and the presence of sideband signals indicates that this interaction had reached a nonlinear stage. The wave magnetic field in the interaction region is estimated to be approximately 20 mγ. The high amplitudes reached by the signals indicates that particle trapping effects could be responsible for the sideband generation.

1. INTRODUCTION

This paper reports new observations in the magnetosphere of nonducted coherent VLF waves from a ground-based transmitter and associated sidebands and VLF emissions. The data reported were acquired by the Stanford University VLF Wave Injection Experiment on the ISEE 1 satellite [*Bell and Helliwell*, 1978]. The experiment has four main components: (1) a broadband (1–32 kHz) VLF receiver on ISEE 1 connected to a long electric antenna, (2) a broadband (1–20 kHz) controllable VLF transmitter located at Siple Station, Antarctica [*Helliwell and Katsufrakis*, 1974], (3) various VLF navigation and communications transmitters, such as those of the worldwide Omega network, and (4) ground stations in the Antarctic and Canada. The main goal of this, and similar experiments, is to understand interactions between coherent VLF waves and energetic particles in the magnetosphere, in particular the whistler-mode instability through which both natural and stimulated VLF emissions are produced [*Helliwell and Katsufrakis*, 1974; *McPherson et al.*, 1974; *Koons et al.*, 1976; *Dowden et al.*, 1978].

Sources of the coherent VLF waves involved in these studies include VLF transmitters, large-scale power grids, whistlers, and other natural coherent VLF signals. Waves injected into the magnetosphere from these sources propagate in either the ducted or nonducted modes. In the ducted mode, the injected waves propagate in ducts of enhanced ionization along paths that are closely aligned with the earth's magnetic field. Near the magnetic equatorial plane, these ducted waves often interact with energetic electrons to produce wave amplification (up to 30 dB), triggering of VLF emissions, and scattering of energetic electrons in pitch angle and energy [*Helliwell and Katsufrakis*, 1974; *McPherson et al.*, 1974; *Dowden et al.*, 1978; *Inan et al.*, 1978; *Bell and Inan*, 1981.]

The injected signals and the associated triggered emissions travel to the ionospheric region conjugate to the source and can enter the earth-ionosphere waveguide to be observed on the ground. On the other end of the field line, the scattered electrons precipitate into the ionosphere causing a variety of perturbations that can be detected from the ground. For example, fluxes of natural VLF wave-induced precipitation have been observed to excite X rays [*Rosenberg et al.*, 1971], photoemissions [*Helliwell et al.*, 1980], and electron density enhancements [*Helliwell et al.*, 1973]. Furthermore, signals from ground-based VLF transmitters have been correlated with precipitating energetic electrons near $L \sim 2$ [*Imhoff et al.*, 1983*a*, *b*].

Although ground-based experiments can determine a number of important features of the interaction, satellite measurements are required to determine the wave and particle properties in or close to the interaction region. In addition, such measurements represent the only means of study-

Paper number 4A8216.
0148-0227/85/004A-8216$05.00

ing the class of injected waves which are nonducted. In general, most of the waves injected by a ground-based transmitter propagate in the magnetosphere in a nonducted mode. Although these waves are capable of strong interaction with energetic particles in the magnetosphere [*Bell et al.*, 1981; 1983*a*], the output of these interactions is not observable on the ground because the nonducted waves generally suffer total internal reflection either due to specular reflection or to magnetospheric reflection [*Edgar*, 1976]. Thus the only means of observing the output of wave-particle interactions involving nonducted injected waves is through the use of satellites (or rockets).

In the present paper, we report new high-altitude ISEE 1 satellite observations of high-amplitude nonducted signals from the Omega navigation transmitter in North Dakota (98°W, 46°N geographic, $L \sim 3.4$). The amplitude of the signals was approximately 16–26 dB higher than that of similar signals observed at comparable locations on other days. The observations reported here were made on February 16, 1983, while the satellite was within 6° of the magnetic equatorial plane, close to the region where it is thought that VLF emissions are generated [*Helliwell*, 1967; *Nunn*, 1974; *Dysthe*, 1971]. As we discuss below, there is good reason to believe that the unusually high amplitude of the observed signals was due to wave amplification through the whistler-mode instability [*Bell and Buneman*, 1964; *Helliwell*, 1967; *Nunn*, 1974; *Dysthe*, 1971].

Sideband signals and VLF emissions associated with the high-amplitude transmitter pulses were also observed, suggesting that a nonlinear stage of the whistler-mode instability had been reached at the time the observations were made. Below, we provide brief background information on the Stanford ISEE 1 wave-injection experiment and follow with a presentation of the data.

2. EXPERIMENT BACKGROUND

Background material concerning the ISEE 1 wave-injection experiment can be found in the literature [*Bell and Helliwell*, 1978; *Helliwell*, 1981]. In brief, one of the main goals of the Stanford ISEE 1 wave-injection experiment is to measure the frequency and amplitude of the injected waves and any associated sideband waves and/or VLF emissions, that are generated as the injected waves propagate through the magnetosphere. In principle, these measurements would serve to determine the location of the VLF wave-particle interaction region where the emissions and sidebands are produced, and could show how the wave amplitude of the injected waves varies with distance through the interaction region.

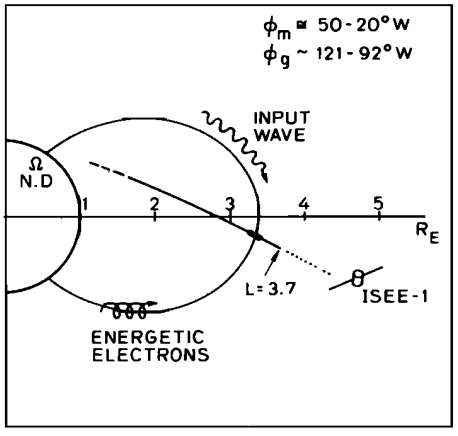

Fig. 1. Schematic representation of the orbital configuration of the ISEE 1 satellite during the period 1620–1720 UT on February 16, 1983. The $L = 3.4$ magnetic shell linking the Omega, N.D. VLF transmitter is shown. The region of high wave amplitude is indicated by a thickened line segment near the intersection of the $L = 3.4$ magnetic shell with the ISEE 1 spacecraft position.

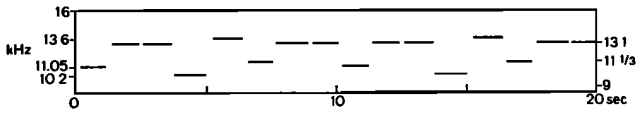

Fig. 2. Two cycles of the Omega North Dakota format. The basic cycle consists of eight fixed-frequency pulses distributed as follows: one pulse at 10.2 kHz with duration 1.1 s, one pulse at 13.6 kHz with duration 1.1 s, one pulse at 11.3 kHz with duration 0.9 s, two pulses at 13.1 kHz with respective durations of 1.2 and 1.0 s, one pulse at 11.05 kHz with duration 0.9 s, and two pulses at 13.1 kHz with respective durations of 1.0 and 1.1 s. Each pulse is separated in time from its successor by 200 ms. The 10-s format is repeated continuously.

The orbital configuration of the ISEE 1 satellite directly following launch (October 1977) was such that the spacecraft crossed the magnetic shell, intersecting the Omega, N. D., transmitter ($L \sim 3.4$) slightly to the south (~5°) of the magnetic equator [*Bell et al.*; 1981; Figure 2]. Thus the spacecraft initially was in an excellent position to observe the injected waves and associated emissions as these signals left the interaction region. Results of these initial observations were reported earlier [*Bell et al.*, 1981]. Due to an increase in inclination, the configuration of the ISEE 1 orbit became less favorable as time progressed and by October 1979, the orbit crossed the L ~3.4 field lines approximately 30° to the south of the magnetic equator, far from the interaction region [see *Bell et al.*, 1981, Figure 2].

A large decrease in orbital inclination during 1982 then led once again to the situation shown in Figure 1, in which the spacecraft crossed the $L \sim 3.4$ magnetic shell just slightly to the south of the magnetic equator. Furthermore, starting in mid-January 1983, the local time of the $L \sim 3.4$ crossings fell within the range 0300-1000 LT, when the injected Omega signals are most likely to trigger VLF emissions [*Bell et al.*, 1981]. Thus the orbital configuration in early 1983 was again very favorable for the wave-injection experiments.

Because of the navigational mission of the Omega transmitter, only the standard modulation format shown in Figure 2 is available for observation by the ISEE 1 satellite. Each 10-s segment has eight fixed-frequency pulses of fixed duration at 10.2 (one pulse), 11.05 (one pulse), 11-1/3 (one pulse), 13.1 (four pulses), and 13.6 kHz (one pulse). Each pulse is separated in time from its successor by 200 ms, and the average pulse length is approximately 1 s.

3. OBSERVATIONS

Signal Amplitude

Signals from the Omega transmitter achieved their highest peak amplitude near 1627:20 UT when the value reached 0.6 mV/m. At approximately the same time, the sidebands

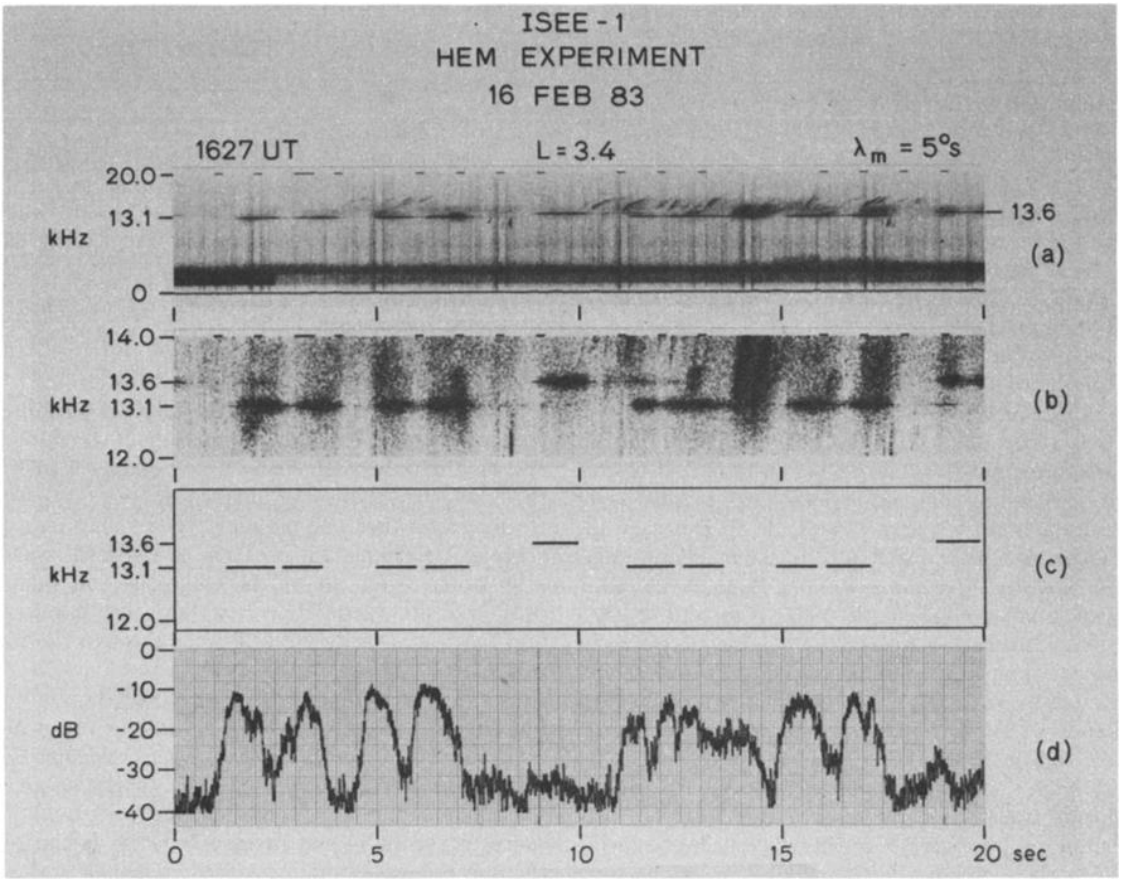

Fig. 3. (*a*) 0–20 kHz spectrogram of VLF wave activity in the region of high-wave amplitude; (*b*) Omega transmitter pulses shown with higher-frequency resolution; (*c*) Omega pulse format; (*d*) chart record of the amplitude of the Omega pulses at 13.1 kHz shown in Figure 3*b*.

associated with each Omega pulse reached their maximum frequency spread of approximately 200 Hz. Spectrograms showing wave data from this period are given in Figure 3. Panel 3*a* shows a 0–20 kHz spectrogram covering a 20-s period centered on 1627:30 UT. At this time only the Omega pulses at 13.1 and 13.6 kHz are in evidence and most of these pulses appear to be associated with weak to moderate intensity rising-tone VLF emissions. The sidebands associated with the pulses can be seen more clearly in panel 3*b*, which shows the same time interval as that shown in 3*a* but with higher frequency resolution. It is clear from 3*b* that the bandwidth of the Omega pulses is of the order of 100 Hz or more and a suggestion of a line structure in the broadened signals can be seen. Panel 3*c* shows the format of the Omega pulses at 13.1 and 13.6 kHz as transmitted, but shifted in time by 0.9 s to allow for the propagation delay from the transmitter to the satellite. The chart recording in panel 3*d* shows the electric field amplitude measured in a 300-Hz band centered on 13.1 kHz.

The amplitude of the electric field of the Omega signals varied markedly during the period of observation, and both short- and long-term variations were present. A short-term variation with a period of ~1.5 sec was associated with the rotation of the electric dipole antenna about the satellite spin axis (see Figure 3*d*). Since whistler-mode waves are generally elliptically polarized, an antenna rotating about a fixed axis in space will measure a wave amplitude which is a function of the antenna orientation angle about the spin axis. Since the polarization of whistler-mode waves is known as a function of wave normal angle [*Helliwell*, 1965], and the ISEE 1 spin axis is known to an accuracy of at least 1°, the short-term spin-dependent wave amplitude variation can be used to estimate the wave normal angle of the observed whistler-mode waves.

In the case of the Omega signals, the ratio between the maximum and minimum electric field amplitudes during each rotation of the dipole antenna was roughly 15 dB during the interval 1627–1629 UT. Examples of this spin fading effect can be seen in Figure 3*d*.

The long-term variation in signal amplitude was much more pronounced than that due to the spin fading effect. Figure 4 shows the wave electric field amplitude at 13.1 kHz as a function of time for the interval 1622–1634 UT. In order to prepare this figure, two measures of amplitude were determined for each 10-s Omega transmitter segment (see Figure 2): (1) a 10-s average peak amplitude, and (2) an average rms amplitude.

The first measure consists of the linear average of the peak amplitudes of the four pulses at 13.1 kHz on each 10-s Omega transmission segment. One such set of four is shown between the 0- and 10-s marks in Figure 3*d*. The second measure consists of the linear average of the RMS amplitudes of the four pulses at 13.1 kHz in each 10-s Omega transmission segment. Use of the 10-s average peak am-

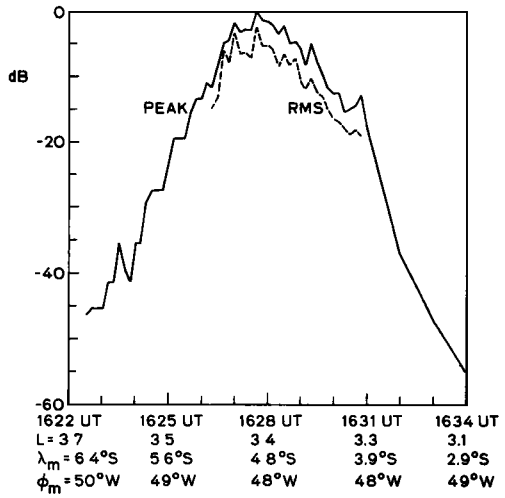

Fig. 4. Average peak amplitude and average RMS amplitude of the Omega pulses at 13.1 kHz during the interval 1622–1624 UT.

plitude substantially eliminates the effects of fading due to antenna rotation. During the period 1626–1630 UT the S/N ratio of the Omega pulses generally lay in the range 20–30 dB, and thus the 10-s average peak amplitude gives a good estimate of the actual signal strength in this interval. Since in practice the dipole antenna will seldom be parallel to the wave electric field along the major axis of the polarization ellipse, the 10-s average peak amplitude represents a lower bound to the actual peak electric field of the Omega signals during any one 10-s period. In cases in which natural VLF noise bursts obscured one or more Omega pulses in a set of four, the average was taken only over the well-defined pulses.

The average rms amplitude includes the effect of spin fading on the measured wave amplitude and represents a lower bound to the actual wave amplitude. The average rms amplitude was determined only over the interval 1626–1631 UT where the natural VLF noise bursts occurred less frequently.

From Figure 4 it can be seen that the average peak amplitude varies over more than a 45-dB range during the interval 1622–1634 UT, with the 0-dB level corresponding to an electric field amplitude of 0.6 mV/m. Peak amplitudes greater than 0.06 mV/m were observed only over a very limited region of space between $L = 3.5$ and $L = 3.3$, a distance of approximately 1200 km. Peak amplitudes before 1023 UT and after 1633 UT were more than 45 dB lower than the maximum value near 1627 UT.

The Omega signal peak amplitude of 0.6 mV/m was the highest Omega amplitude observed to date by the Stanford University experiment on the ISEE 1 satellite, exceeding commonly observed amplitudes in this region by 16–26 dB [*Bell et al.*, 1981].

Sideband Characteristics

Sidebands of significant amplitude (above noise) were associated with the Omega transmitter signals from 1626–1630 UT. Figure 5 shows two spectrograms of data acquired during the period. The upper spectrogram shows Omega signals at 13.1 kHz accompanied by hisslike sidebands extending roughly ±100 Hz about the signal frequency. The lower spectrogram shows a portion of the data with higher frequency and time resolution, and some structure can be seen in the sidebands.

The sideband structure is brought out more clearly in Figure 6, which shows signal amplitudes as a function of frequency and time for three Omega pulses associated with sidebands. The amplitude is shown across a 330-Hz frequency range which includes the frequency of the Omega pulses at 13.1 kHz. Each spectral scan is carried out in 8 ms and scans are repeated every 50 ms. Approximately 250

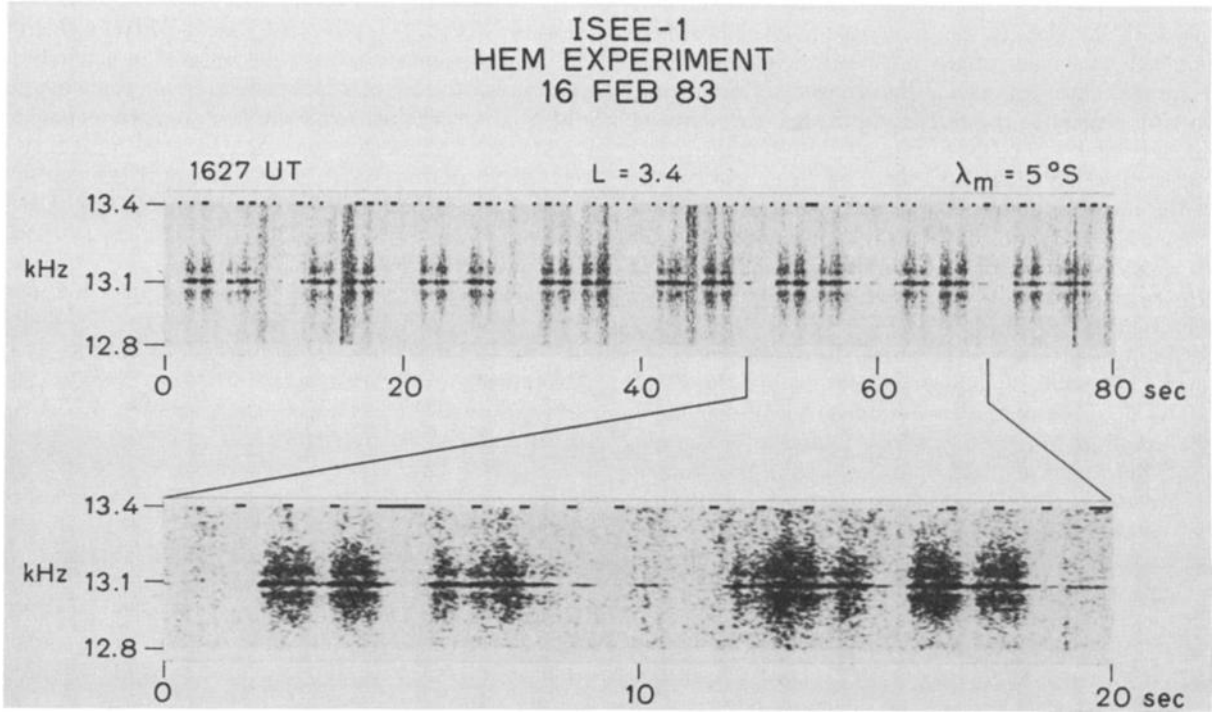

Fig. 5. High-frequency resolution spectrograms of the Omega pulses at 13.1 kHz in the region of high amplitude.

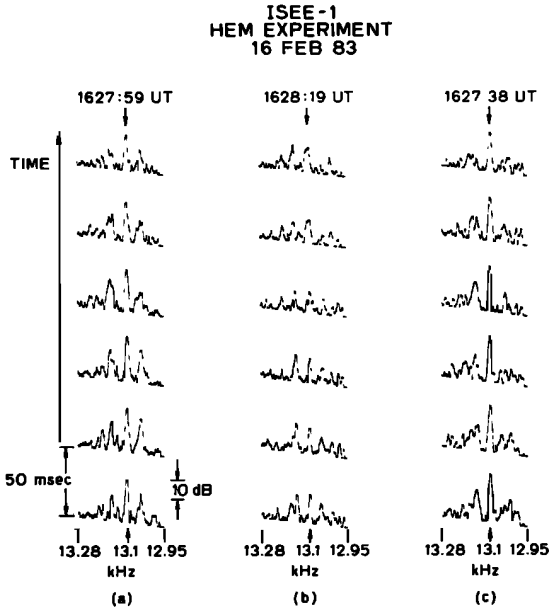

Fig. 6. Wave amplitude scans showing the Omega signal amplitude as a function of frequency. Note that the frequency decreases toward the right on the frequency axis.

ms of data are shown for each pulse. The amplitude on each scan is measured on a logarithmic scale with respect to the sloping baseline. The position of the Omega signal is indicated by an arrow perpendicular to the frequency axis. In most cases there is a good deal of structure to the sidebands which is not readily apparent from the spectrograms of Figure 5.

Panel 6*a* illustrates a case in which the main sidebands are approximately the same amplitude and are located roughly symmetrically about the carrier (the Omega signal) at 13.1 kHz. The amplitude of the main sidebands is approximately 5 dB below the carrier. In the first three amplitude sweeps the main sidebands are sharp and well-defined, and are spaced approximately ± 55 Hz (measurement uncertainty ± 4 Hz) with respect to the carrier. In the last three sweeps the main sidebands are broader in bandwidth but the center frequencies of the sidebands are still offset by approximately ±55 ±4 Hz from the carrier. The second sweep clearly shows the presence of secondary sidebands at approximately 38, 93, and 110 Hz above the carrier. No similar sidebands are seen below the carrier. Secondary sidebands are present in all six sweeps at varying amplitude levels.

Panel 6*b* illustrates a case in which the amplitude of the main upper sideband is comparable to, or slightly higher than, the amplitude of the carrier, and ~5–10 dB higher than the amplitude of the main lower sideband. The amplitude of the carrier in panel 6*b* is down by approximately 10 dB from the carrier signal shown in panel 6*a*. For the six sweeps shown, the spacing between the carrier and main upper sideband stays roughly constant at 50 ± 4 Hz, while the spacing with respect to the main lower sideband is variable. In the first three sweeps, two subsidiary sidebands in addition to the main lower sideband at 44 ± 4 Hz can be seen at frequencies of 88 ± 4 Hz and 121 ± 4 Hz below the carrier. In the last two sweeps, the sideband at 44 ± 4 Hz below the carrier has decreased significantly in amplitude so that the sideband at 88 ± 4 Hz has become the main lower sideband.

Panel 6*c* illustrates the case in which the carrier was generally significantly higher in amplitude than the sidebands. In the case shown the main upper sideband is generally higher in amplitude than the main lower sideband. Separation between the main upper sideband and the carrier varies between 55 ± 4 Hz (first four sweeps) to 66 ± 4 Hz (last two sweeps). Cases in which the main lower sideband was dominant were also common.

The sidebands were most easily detected during the period of high wave amplitude when the S/N ratio of the pulses was high. However, in general, sidebands were associated with the Omega signals throughout the entire region, $3.3 \leq L \leq 3.7$. As shown in Figure 4, the signal amplitude over this region varied by more than 40 dB. Thus high amplitudes were not a necessary requirement for the appearance of sidebands. In the lower amplitude region, $3.5 \leq L \leq 3.7$, the S/N ratio of the pulses was not sufficient to resolve the sidebands completely but in general the main sidebands, when observable, were separated from the carrier by $\sim \pm 55 \pm 4$ Hz. Thus the main sideband spacing was independent of the amplitude of the carrier over a 40 dB amplitude range. This result suggests that the sidebands were not generated locally.

During the period of high wave amplitude the differential time delay between the carrier and the main sidebands was generally less than 100 ms, and the differential delay between the two main sidebands was generally less than 10 ms.

General Features of the Data

The event of February 16, 1983 can be divided into four distinct stages, and data from the first three of these are shown in Figure 7. Panel 7*a* shows a 0–16 kHz spectrogram of electric field wave data acquired at $L \sim 3.6$ and λ_m (magnetic latitude) $\sim 6°$ S shortly after the Omega signals were first observed. In this stage, Omega pulses at all five frequencies (10.2, 11.05, 11.3, 13.1, and 13.6 kHz) were present. The Omega signals at this time lay within a band of natural emission activity which extended approximately from 8–14 kHz. Occasional weak whistlers were observed to trigger strong VLF emissions above the whistler nose frequency. An example of this type of event occurs at the arrow marked W near 2.5 s. In addition to the strong VLF emissions, a weak noise band between 13 and 14 kHz is also triggered which endures for at least 5 s. Near the 7.5-s mark (see arrow marked E1), a transmitter pulse at 13.1 kHz appears to trigger a burst of strong rising-tone VLF emissions, and near the 15-s mark (see arrow marked E2) a pulse at 11-1/3 kHz appears to trigger a series of strong rising-tone emissions and hisslike noise lasting approximately 4 s. Although the emissions and transmitter pulses appear to be strong in the spectrogram, the receiver was operating at high gain and the peak amplitude of the transmitter pulses was less than 6 μV/m.

Panel 7*b* shows wave data during the second stage of development in which the band of natural emission activity has narrowed to the 12–14 kHz range. Arrows marked E1 and E2 along the time axis show the location of two whistler triggered noise bursts within the emission band. In this stage only the Omega pulses whose frequencies lay within the natural noiseband were observable and these pulses were asso-

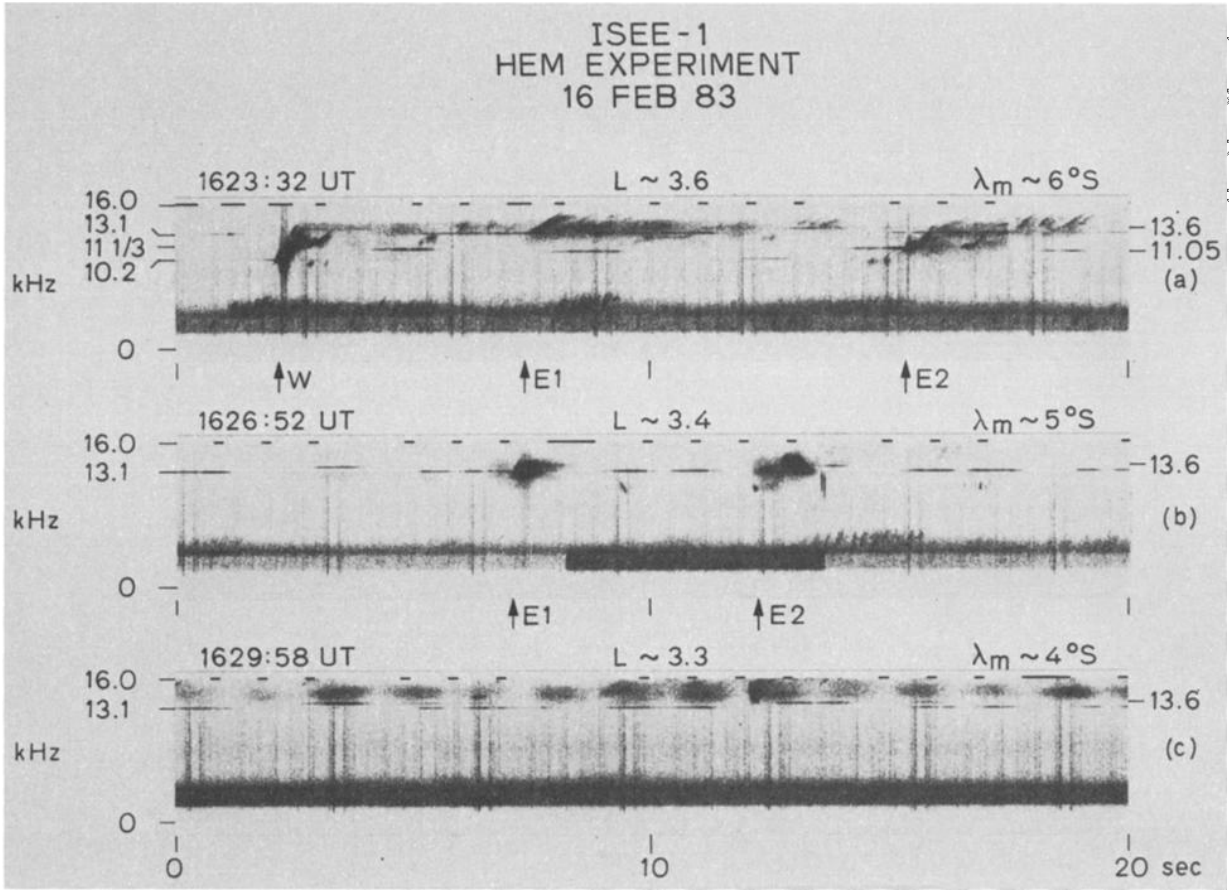

Fig. 7. Spectrograms of the VLF wave activity observed on the ISEE 1 spacecraft on 16 February, 1983.

ciated with sideband signals of generally lower amplitude. At this time the receiver was in its lowest gain state and the peak amplitude of the transmitter pulses reached values as high as 0.6 mV/m. Data from this second stage has been discussed in sections 3.1 and 3.2 above.

Panel 7*c* shows wave data during the third stage of development in which the band of natural emission activity had risen to frequencies (14–16 kHz) above those of the transmitter pulses. At this time the natural emissions consisted generally of bursts of hisslike noise. The peak amplitude of the Omega pulses had dropped below 0.1 mV/m, and continued to decrease as the natural noise band rose higher in frequency. After ~1 min the pulse amplitude had decreased to the point that the pulses were no longer detectable in the data. Within the next 3 min the natural noise band gradually weakened and the receiver gain became high enough that the Omega pulses were once again detectable in the data and this situation continued for the next 30 min. This fourth stage in development is illustrated in Figure 8.

Panel 8*a* shows an 8–18 kHz spectrogram of data from the initial portion of the fourth stage when the Omega pulses had once again become detectable in the data. Although Omega pulses at all frequencies are present in the data, only pulses at 13.1 and 13.6 kHz are associated with the bursts of rising-tone emissions and hisslike noise that extend up to 18 kHz. The peak amplitude of the Omega pulses at this time was less than 20 μV/m. Panel 8*b* shows the wave data somewhat later near the geomagnetic equator. At this location only pulses at 13.6 kHz were seen to trigger VLF emissions. Panel 8*c* shows the wave data at a location 3°N of the geomagnetic equator, where pulses at 13.6 kHz were associated with strong bursts of rising-tone VLF emissions. Weaker triggering by pulses at 13.1 kHz is also evident. The triggered emissions of panel 8*c* resemble closely those of panel 8*b*. Panel 8*d* shows the wave data at a location 9°N of the geomagnetic equator at $L \sim 2.2$. Bursts of rising-tone emissions resembling those of panel 8*b* are again associated with transmitter pulses at 13.6 kHz.

The initiation of transmissions at 13.6 kHz occurred at times $t = 0$ and 10 s in each panel. The propagation delay of the pulses at 13.6 kHz varied approximately linearly with time from 0.7 s in panel 8*a* to 0.3 s in panel 8*d*. In contrast, the delay of the triggered rising-tone emission bursts (with respect to the transmission initiation times) at 13.6 kHz remained relatively constant at 1.3 ± 0.1 s. The nominal duration of the pulses at 13.6 kHz is 1.1 s while the observed duration in all panels exceeds 2 s. This indicates that the pulses were propagating to the satellite along at least two paths of significantly different time delay.

Natural Noise Band

High-amplitude Omega signals and associated sidebands were observed only during the time that the frequency of these signals lay within a band of natural noise and emission activity. Examples of this natural noiseband and the natural emissions triggered within it are shown in Figure

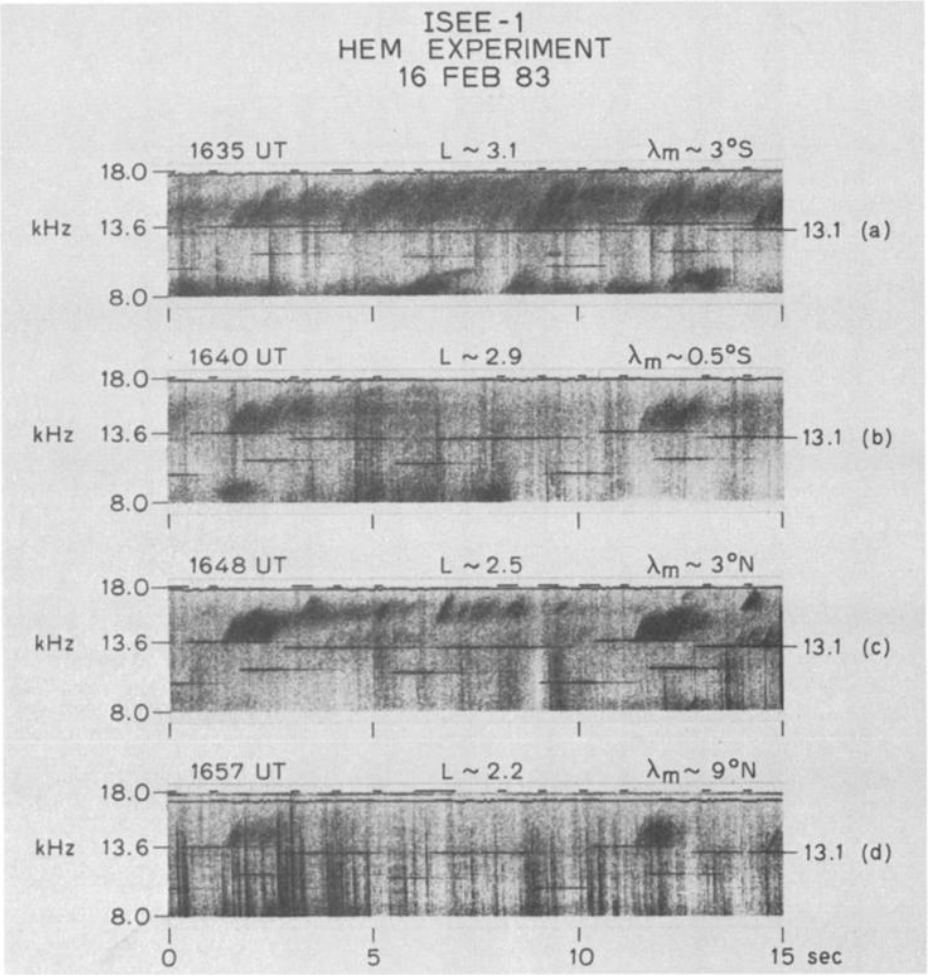

Fig. 8. Spectrograms of the VLF wave activity observed on the ISEE 1 spacecraft on February 16, 1983.

7. Many of the natural emissions in this noise band appeared to have been triggered by whistlers, and these emissions were generally higher in amplitude than the Omega signals received at or near the same time. For instance, Figure 7*b* shows two strong natural noise bursts (initiation times labeled E1 and E2) whose peak amplitudes in a 300-Hz band centered on 13.1 kHz exceeded that of the nearby Omega signals by ~5 dB. Assuming these signals have propagated along the same path, it appears that the amplitude of Omega signals was not limited by high-amplitude saturation of the whistler-mode amplification mechanism but instead was possibly limited by the sidebands, whose presence could cause suppression of the growth [*Chang and Helliwell*, 1980].

Natural whistler mode noise bands outside the plasmasphere near the magnetic equatorial plane are often observed to consist of two parts; a narrow band of emission with an upper cutoff frequency slightly below one half of the local electron gyrofrequency (f_H) and a narrow band with a lower cutoff frequency slightly above $f_H/2$ [*Burtis and Helliwell*, 1976; *Anderson and Maeda*, 1977; *Hashimoto and Kimura*, 1981.

In general, during the period of highest Omega signal amplitude the lower cutoff frequency of the natural noise band exceeded one half of both the local and equatorial electron gyrofrequencies by ~1–2 kHz. In this respect the noise band is similar to the upper band commonly observed outside the plasmasphere. However, it may be more closely related to the noise band observed outside the plasmasphere in the frequency range $f_H/2 < f < f_H$ during periods of enhanced low energy (1-10 keV) electron fluxes [*Anderson and Maeda*, 1977].

Pulse Time Delay

Figure 9 shows the group time delay of the Omega (N.D.) pulses at 10.2, 11.33, 13.1 and 13.6 kHz plotted as a function of universal time and satellite position. The group time delay is defined here as the difference between the transmission time of the leading edge of a particular pulse and the time at which this leading edge was received on the satellite.

The reception time of the leading edge of each pulse was assumed to be the time at which the pulse amplitude S/N ratio in a 300-Hz bandwidth centered on the carrier frequency first exceeded 10 dB. In order to minimize errors, the delay time plot does not include pulses whose leading edges were obscured by the spin fading effect shown in Figure 5*d*.

To improve clarity, the measured time delay values of the pulses at 13.1 kHz are shown connected by solid lines. The measurement accuracy of all points is ±50 ms. The time delays of the pulses at 11.05 kHz are not shown, since these

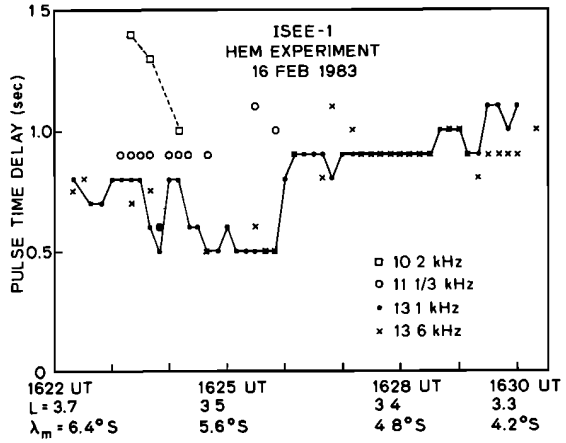

Fig. 9. Group time delay of the Omega pulses at 10.2, 11 1/3, 13.1 and 13.6 kHz shown as a function of time and satellite position.

were generally identical to those of the pulses at 11.33 kHz.

Initially (1622 UT), Omega pulses at all five frequencies were received on the satellite but the time delay could be measured only for the pulses at 13.1 and 13.6 kHz. Near 1623 UT the S/N ratio of other pulses improved and time delay measurements were made on all pulses. Delays ranged from 1.4 s at 10.2 kHz to 0.7 s at 13.6 kHz. After 1623 UT the time delays at 13.1 and 13.6 kHz began to decrease toward 0.5 s and the amplitude of the pulses at 10.2 kHz dropped below the natural noise level. Between 1625:30 UT and 1626:20 UT, the time delay of the pulses at 13.1 and 13.6 kHz increased abruptly from 0.5 s to 0.9 s. Simultaneously the amplitude of the pulses at 11.05 and 11.33 kHz dropped below the natural noise level. During the period of high wave amplitude, 1626–1629 UT, the time delays of the pulses at 13.1 and 13.6 kHz were generally identical at $\sim 0.9 \pm 0.05$ s.

The received signal in the period 1624:30 to 1625:50 UT consisted of two parts, a component propagating along a short time delay path ($\sim$ 0.5 s) and a component propagating along a longer time delay path ($\sim$ 0.8 s). The longer time delay path is thought to be closely related to the path associated with the pulses received both before and after the short time delay period.

According to Figure 4, the amplitude of the signal propagating along the short time delay path was $\sim$ 20 dB below the maximum level. Thus the apparent absence of this path for the period following 1626 UT could be caused by the limited dynamic range of the receiver.

Cold Plasma Distribution

During the period of observation of the Omega, N.D. pulses, simultaneous plasma wave data was obtained by the University of Iowa ISEE 1 sweep frequency receiver (Gurnett, 1978). The sweep frequency receiver data generally allows very accurate sheath-independent measurements to be made of the natural noise bands which occur between the upper hybrid-frequency and the plasma frequency through much of the ISEE 1 orbit. From measurement of the upper-cutoff frequency of the upper-hybrid noise band, it is generally possible to estimate the local cold plasma density to within a few percent inside the plasmasphere. Unfortunately, due to enhanced levels of natural background noise on February 16, it was at times difficult to identify the upper hybrid noise band. Thus the cold plasma density estimates were at times subject to considerable uncertainty.

In Figure 10, we show the cold plasma density profile derived from the University of Iowa data for the time period 1600–1700 UT. (These data were provided by R. Anderson.) It is clear from the figure that during the time of observation the plasmapause was located near $L = 3$, well inside its average position near $L = 4$. This inward position was presumably related to the high level of magnetic disturbance which existed prior to, and during, the time of observation.

The three hour planetary geomagnetic index Kp during the time of observation had the value 5- and the maximum Kp during the preceding 12 hours was 5+. According to *Carpenter and Park* [1973], this level of geomagnetic activity would, on the average, result in a plasmapause position at $L \sim 3.3$, a value very close to that shown in Figure 10.

The figure indicates the region of high wave amplitude ($3.3 \leq L \leq 3.5$)and the region ($2.2 \leq L \leq 3.1$) in which strong VLF emissions were associated with the Omega pulses. It is interesting that the side band generation occurred outside the plasmapause while the emission triggering for the most part occurred inside the plasmapause. Further comments on this situation are included below.

4. Interpretation and Discussion

Propagation Mode

The peak amplitude of the Omega, N. D., signals reached a value of 0.6 mV/m at 1627:30 UT when the magnetic longitude of the ISEE 1 satellite was ~48° W, approximately 10° west of the magnetic meridian of the Omega, N. D., transmitter (~35° W). The L shell of the satellite at this time was $L \sim 3.4$, very close to the L shell which intersects the transmitter location.

Typical peak intensities of Omega, N. D., signals in this region of the magnetosphere at similar local times lie in the range 0.03–0.1 mV/m (see Figure 9 of *Bell et al.* [1981]). Thus the peak amplitudes of the Omega signals on February 16 exceed the typical values by 16–26 dB. We conclude that the ISEE 1 satellite was detecting transmitter signals which had propagated through a magnetospheric "hot spot" or VLF wave amplification "cell" in which coherent VLF waves in a narrow band of frequencies were being amplified through the whistler-mode instability. It is noteworthy that

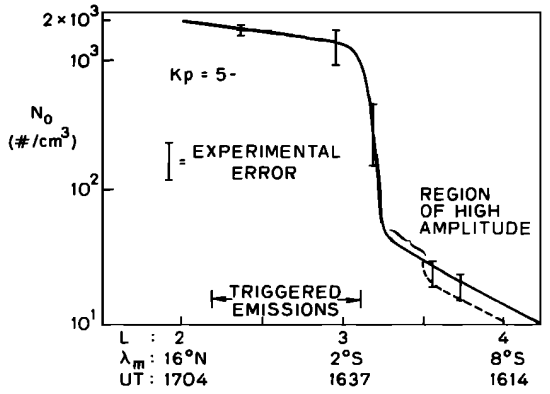

Fig. 10. Magnetospheric cold plasma density as derived from the University of Iowa instrument on ISEE 1 on February 16, 1983.

the S/N ratio of the Omega signals in the high amplitude region was at least 20 dB (see Figure 4*d*). Thus the natural incoherent VLF background noise was not amplified to the same level as the coherent signals. This disparity between amplified (presumably) incoherent background noise levels and the levels of amplified coherent signals is typical of that observed in ground-to-ground wave injection experiments [*Helliwell and Katsufrakis*, 1974].

The spatial distribution of wave amplitude as shown in Figure 4 is sharply peaked near $L \sim 3.4$, with the -20 dB peak amplitudes being located approximately at $L = 3.4 \pm 0.1$. Thus the highest amplitudes are located in a region of radial cross section of ~1200 km. This cross section is comparable to that deduced for the cross section of whistler-mode ducts [*Angerami*, 1967] of enhanced ionization. However, there are at least two reasons for believing that the high amplitude transmitter pulses were not ducted. First, during the time the highest wave ampitudes were recorded (1625–1630 UT), the electron gyrofrequency at the satellite location lay in the range 21–25 kHz. Thus the frequency of the Omega signals at 13.1 and 13.6 kHz exceeded one-half of the local electron gyrofrequency and in theory could not have been trapped in a duct of enhanced ionization [*Helliwell*, 1965]. However, trapping in a depletion duct would in principle still be possible [*Helliwell*, 1965].

Second, the amplitude of the Omega signals exhibits a deep fading with a period of one-half of the satellite spin period as the dipole antenna rotates about the spin axis (which is always closely perpendicular to the ecliptic plane). If the wave normal of the Omega signals is locally parallel to the earth's magnetic field $\mathbf{B}_0$, the signals will be circularly polarized, and it can be shown that the ratio R of minimum to maximum wave amplitude during one spin period will have the value $R = \cos\gamma$, where γ is the local angle between $\mathbf{B}_0$ and the satellite spin axis. During the interval 1622–1634 UT, γ was less than 15°, and the predicted spin-fade would be less than 1 dB for a circularly polarized wave. However, the measured spin-fade was approximately 15 dB. Thus we conclude that the Omega signals were not circularly polarized and that their wave normals were not parallel to $\mathbf{B}_0$.

Furthermore, using well-known relations for the polarization of whistler-mode waves as a function of wave normal angle [*Helliwell*, 1965], in conjunction with the measured value of the spin-fade of the Omega pulses, it can be shown that a wave normal angle of 35°–45° is consistent with our observations. This inferred wave normal angle is comparable to the resonance cone half-angle which at 13.1 kHz at 1627 UT had the approximate value of 54°. A wave normal angle of this magnitude is not consistent with that associated with trapping in a depletion duct [*Helliwell*, 1965]. Thus we conclude that it is unlikely that the high amplitude signals were propagating in either a depletion or enhancement duct in the region of observation.

Figure 7*a* shows an example of the type of whistler which was frequently detected on the ISEE 1 satellite during the period 1622-1627 UT. In general these whistlers possessed frequency components well above one-half of the local gyrofrequency (f_H) and were observed to trigger VLF emissions and noise bands at frequencies also well above $f_H/2$.

These characteristics are similar to those of a type of whistler commonly observed in data from ground stations and labelled "knee trace" (KT) whistlers [*Carpenter*, 1978]. The KT whistlers have been shown to propagate just beyond the plasmapause in the low density or plasma trough region. The unusual features of these whistlers include frequency components up to 0.8 f_{Ho} where f_{Ho} is the minimum gyrofrequency along the magnetic field line of propagation, and a tendency to trigger noise bands and bursts in the frequency range 0.4–0.8 f_{Ho} [*Carpenter*, 1978].

In view of these similarities it is suggested that the whistlers detected on ISEE 1 were actually KT whistlers which had originally propagated along the base of the plasmapause into the southern ionosphere, from which point they had reflected or scattered back up to the satellite.

Since the Omega signals possessed high amplitudes only when they were located within the noise band triggered by the whistlers, it is possible that the Omega signals propagated along the same path as the KT whistlers and reached their high amplitude as a result of the whistler mode instability.

The nose frequency of the KT whistlers was approximately 10 kHz. This value is consistent with a propagation path near $L \sim 3.3$ close to the base of the plasmapause (see Figure 10).

If the Omega signals did indeed propagate within the KT whistler duct into the southern hemisphere and reached the satellite only after reflection from the southern hemisphere, then the observed amplitude distribution of the Omega signals would be a result of the reflection process rather than the amplification process. Furthermore, if the sidebands are generated within the duct during the wave amplification process, the sideband spacing would reflect only conditions in the duct. Thus the lack of dependence of sideband spacing on the wave amplitude as measured on the satellite would not be surprising.

An alternate possibility is that the Omega signals did not propagate into the southern hemisphere in a duct but instead followed a nonducted, or partially nonducted path. In order to test this hypothesis, a ray tracing study was carried out using a model magnetosphere based upon the cold plasma density profile of Figure 10. The details of the ray tracing study are given in the appendix. This study indicates that the high amplitude Omega signals could have reached the satellite with the observed time delay and appropriate wave normal angle through the following four step process:

1. The waves are injected into the ionosphere in the northern hemisphere near $L \sim 3$, with vertical wave normals. They then propagate in a duct of enhanced ionization along the $L = 3.5$ magnetic shell from 1000 km altitude up to ~ 14,800 km altitude and ~ 13°N magnetic latitude where the wave frequency is approximately equal to the duct upper cutoff frequency at one half of the local electron gyrofrequency.

2. The waves then exit from the duct and propagate in the nonducted mode inward to the base of the plasmapause at $L \sim 3.3$.

3. Guided propagation along the base of the plasmapause then takes place until the waves reach the conjugate ionosphere near $L \sim 3$. Wave guidance along the base is analogous to that which takes place in a depletion duct [*Inan and Bell*, 1977].

4. A portion of the waves guided into the conjugate hemi-

sphere are reflected at lower altitude (< 1000 km) and propagate back up to the satellite location near $L \sim 3.4$. A reflection could take place through either a specular reflection in the ionosphere or a magnetospheric reflection [*Edgar*, 1976].

A sample ray trajectory following this propagation path is illustrated by rays V and VI of Figure A1*b*. In this model, nearly all of the Omega signals observed on the satellite outside the plasmapause would be reflected from the southern hemisphere; the single exception to this rule being the relatively weak signals which propagated along a direct path similar to that of ray III of Figure A1*b* and arrived at $L \sim 3.5$ with a time delay of ~ 0.5 s. Thus the amplitude variation of the Omega signals shown in Figure 4 would be related to the reflection or backscatter process rather than the whistler mode amplification process.

The two propagation models proposed above have a number of uncertainties. For instance as a result of the high level of magnetic disturbance, the natural noise background level at the three ground stations, Roberval (Quebec), Siple (Antarctica) and Palmer (Antarctica) was elevated to the extent that no whistlers were observable in the VLF wave data. Thus it could not be established that whistlers such as those shown in Figure 7 were genuine KT whistlers. Futhermore, the atmospheric noise bursts associated with the lightning impulses which initiated these whistlers could not be identified. Thus the group time delay of the whistler frequency components at 13.1 and 13.6 kHz could not be compared with the group time delay of the Omega signals at these frequencies in order to provide evidence that these signals had propagated over the same path.

Furthermore, the data provides no information concerning the reflection mechanism in the southern ionosphere, and thus both models are lacking in this regard.

In addition it is not clear that the two models are actually different since it is not known how KT whistlers propagate between hemispheres. However it should be noted that the ray tracing study described in the appendix does not provide a complete explanation of KT whistler propagation, since the waves associated with ray V of Figure A1*b* arrive at the D region boundary with wave normals nearly perpendicular to $\mathbf{B}_o$ and thus will not be transmitted to the ground [*Helliwell*, 1965]. Transmission to the ground could possibly occur if there exist strong horizontal gradients in cold plasma density which can rotate the wave normal to a vertical orientation during propagation below 1000 km. Strong horizontal gradients are known to exist in the low altitude plasma trough region near the base of the plasmapause [*Ahmed et al.*, 1979]. However, the inclusion of these gradients in a ray tracing study is beyond the scope of the present paper.

Despite the uncertainties associated with the propagation models, either can successfully explain the observed time delays of the Omega signals and their distribution over the satellite track.

According to Figure 10, the spacecraft crossed the base of the plasmapause sometime near 1632 UT, at a magnetic latitude of $\sim 4°$S, and at this time the measured wave amplitude was ~ 20 dB below the maximum levels near 1627 UT (see Figure 4). This circumstance suggests that the satellite did not penetrate the region of wave amplification at the base of the plasmapause, possibly because the amplification region was located at latitudes greater than 4°S or because it was located at a magnetic meridian different from that of the satellite.

The east-west dimension of the duct structure that guides KT whistlers between hemispheres has been estimated to lie in the range of 200 to 500 km at ionospheric heights [*Carpenter*, 1978]. This corresponds to a longitudinal width of approximately 4° to 10° in the magnetic equatorial plane at $L \sim 3.3$. These dimensions are comparable to those estimated by *Angerami* [1970] for ducts of enhanced ionization.

The ISEE 1 satellite was located approximately 13°W of the magnetic meridian of the Omega, N.D. transmitter during the time that the highest signal amplitudes were observed, thus it is possible that the KT whistler duct could have been located close enough to the transmitter meridian that the satellite did not penetrate the region of wave amplification as it crossed the base of the plasmpause.

If it is true that the wave amplification and side band generation took place in a generation region near the equatorial plane at the base of the plasmapause, then the maximum amplitude of the Omega signals measured on the spacecraft could be much lower than that in the generation region due to wave spreading losses, as well as losses due to absorption and scattering in the ionosphere.

The wave energy loss would depend upon the reflection or backscatter mechanism. If the reflection were of the magnetospheric (MR) type [*Edgar*, 1976], it would take place at relatively high altitude and very little spreading loss or absorption loss would be expected. However, for magnetospheric reflection to occur the wave frequency must be less than the maximum lower-hybrid-resonance frequency along the ray path and the LHR frequency rarely exceeds 5 kHz outside the plasmasphere. Thus magnetospheric reflection appears unlikely.

A more likely mechanism is reflection from the lower ionosphere. Under quiet conditions, *D* region absorption at 0800 LT for vertically incident waves at 13.1 kHz would be at least 20 dB [*Helliwell*, 1965]. However under disturbed conditions such as existed on February 16 the absorption losses could be much larger.

Absorption losses would be reduced if the waves are backscattered from irregularities in the *E* region (sporadic *E*). Wave spreading losses would also be minimized if the irregularities were horizontally stratified with a horizontal scale large compared to the signal wave length. Such irregularities could possibly have been produced through enhanced precipitation of energetic electrons from the magnetosphere during the period of magnetic disturbance. The reflection coefficient of this type of irregularity could be reasonably large. For instance consider the simple model in which a 13.1 kHz whistler mode wave is vertically incident on a sharply bounded horizontal surface across which the electron density changes from N to αN. If we assume $\mathbf{B}_o$ is approximately vertical, it can be shown that the reflection coefficient for the wave electric field has the approximate form: $E_r/E_i = (1 - \alpha^{1/2})/(1 + \alpha^{1/2})$ where E_r and E_i are the reflected and incident components respectively. For a 4 to 1 increase in density, $\alpha = 4$, and approximately 10% of the incident wave energy will be reflected.

Sideband Generation

The spectral distortion of multipath signals from VLF transmitters due to the Doppler effect on satellites is a common phenomenon which has been reported by a number of

workers [*Walter and Angerami*, 1969; *Cerisier*, 1973; *Koons et al.*, 1974; *Edgar*, 1976; *Bell et al.*, 1983*b*]. In this effect fixed frequency signals propagate to the satellite along a number of separate paths and arrive at the satellite with different values of refractive index and wave normal direction. Due to their differing Doppler shifts, these signals appear to be separated in frequency on the moving satellite, and apparent sideband structures can be created.

The bandwidth $\Delta\omega$, of the fixed frequency signal as observed on the satellite is given by the Doppler relation $\Delta\omega = \delta\mathbf{k}\cdot\mathbf{V}$, where $\mathbf{V}$ is the satellite velocity and $\delta\mathbf{k}$ is the spread in wave number. Two types of spectral distortion have been reported. One type, involving interhemispheric propagation, is generally characterised by sidebands which are not symmetric in frequency about the carrier and by differential time delays between carrier and sidebands which can be as large as one second [*Walter and Angerami*, 1969; *Cerisier*, 1973; *Koons et al.*, 1974; *Edgar*, 1976.]

The second type, seen predominantly on short propagation paths (< 6000 km), apparently involves the scattering of signals from irregularities in the ionosphere, and is generally characterized by sidebands symmetric about the carrier, differential time delays of approximately 150 ms or less, and a unique "chevron" spectral form [*Bell et al.*, 1983*b*].

The sidebands observed on February 16 did not exhibit the characteristics of either of the two types of spectral distortion discussed above.

Using the expression for the whistler mode refractive index [*Helliwell*, 1965] it can be shown that if the sidebands at ±55 Hz were produced through a Doppler shift effect, then the refractive index, n, and group velocity, v_g, of the sideband signals must satisfy the relation: $n \geq 300$ and $v_g \leq c/200$. Furthermore it can be shown that for the carrier: $n \simeq 8$ and $v_g \cong c/10$. The differential time delay between carrier and sidebands on February 16 was generally less than 100 ms. Thus if the sidebands were produced through a Doppler shift effect, then the values of group velocity given above for the carrier and sideband waves indicate that the sideband waves would have to have been generated within 150 km of the spacecraft. Local generation of sidebands does not appear to be a viable explanation in view of the constancy of the sideband frequencies over the range $3.3 \leq L \leq 3.7$ where the local magnetic field and cold plasma density are known to vary significantly. Instead it appears more reasonable to assume that the sidebands were generated in a whistler mode duct, propagated into the southern hemisphere, and subsequently scattered back up to the satellite location.

The magnetospheric generation of sidebands around an initially monochromatic VLF input wave is strong evidence for the nonlinear nature of the interactions in the magnetosphere between energetic electrons and coherent VLF waves. A number of ground-based observations of sideband generation in VLF transmitter signals propagating through the magnetosphere in whistler mode ducts have been reported in the past [*Bell and Helliwell*, 1971; *Likhter et al.*, 1971; *Park and Chang*, 1978; *Helliwell*, 1979; *Chang et al.*, 1980; *Park*, 1981].

This process of sideband generation has been referred to as the whistler mode sideband instability and a number of theoretical treatments of this instability have been given for the case of ducted monochromatic whister mode waves [*Das*, 1968; *Brinca*, 1972; *Budko et al.*, 1972; *Nunn*, 1973, 1974; *Newman*, 1977; *Lashinsky et al.*, 1980].

In general, theory predicts that the sidebands are generated when energetic gyroresonant electrons become trapped in the potential well of whistler mode waves and the distribution function of the energetic particles becomes distorted. In general, in the early stages of evolution of the system, the frequency separation Δf between the large-amplitude input signal and the sidebands is proportional to $(B_w)^{1/2}$, where B_w is the wave magnetic field amplitude. According to *Brinca* [1972], the sideband separation has the approximate value

$$\Delta f \simeq \pm\frac{2}{\pi^2} < \omega_T > [1 + \frac{\omega_H}{2\omega}]^{-1} \tag{1}$$

where ω is the angular frequency of the input wave, ω_H is the angular gyrofrequency of the resonant trapped electrons, and $< \omega_T >$ is the ensemble average of the nonlinear trapping frequency ω_T. The expression for ω_T has the form

$$\omega_T = [\omega_w k v_\perp]^{1/2} \tag{2}$$

where $\omega_w \equiv \xi B_w$, ξ is the charge-to-mass ratio of the resonant electrons, k is the wave number of the input wave, and $v_\perp$ is the velocity of the resonant electrons perpendicular to $\mathbf{B}_0$. Using the gyroresonance relation $v_{||} = (\omega_H - \omega)/k$, (2) can be written in the equivalent form

$$\omega_T = [\omega_w(\omega_H - \omega)\tan\alpha]^{1/2} \tag{3}$$

where α is the resonant particle pitch angle.

Expressions similar to (1) and (2) have also been derived independently by *Budko et al.* [1972]. In general, sidebands were observed with the Omega pulses over the interval 1623–1631 UT. Throughout the period of observation, the spacing of the main sideband components remained constant at roughly 55 Hz, even though the wave electric field amplitude varied by 40 dB. We believe that this lack of dependence of sideband spacing upon local wave amplitude supports the hypothesis that the sidebands were not locally generated, but had propagated to the region of observation from some distant generation region, near the base of the plasmapause. (However, it should be noted that ground based observations suggest that the sideband spacing may not depend strongly upon the carrier amplitude [*Park*, 1981].)

Assuming that Brinca's theory of sideband generation is correct and that the waves in the interaction region are propagating approximately along B_o, we can use (1) to estimate the wave magnetic field in the region of sideband generation. Using $\Delta f \sim 55$ Hz we find

$$B_w \simeq 23/\eta^2 \quad m\gamma \tag{4}$$

where $\eta = < (\tan\alpha)^{1/2} >$.

The quantity η cannot be calculated directly since no energetic particle data was available during the period of observation. However, the amplification of signals from the Siple Station VLF transmitter has been associated with a "pancake" or "loss cone" type of energetic electron distribution function. Thus, we estimate η by assuming that a loss-cone type of energetic electron distribution function, i.e., $F(\mathbf{v}) \sim \sin^m\alpha/v^p$, exists in the interaction region near $L \sim 3.3$. For the case of propagation along B_o, the signals at 13.1 and 13.6 kHz would resonate with energetic electons of approximately 10 keV in kinetic energy parallel to B_o. For this energy, according to *Anderson and Maeda* [1977], $p \sim 4$ and $m \sim 1$ near the plasmapause boundary. For these values $\eta \sim 1.2$ and theory predicts that $B_w \simeq 16$ mγ.

On the other hand the measured local cold plasma density within the high amplitude region was ~ 40 cm^{-3} and the inferred wave normal angle was $\sim 45°$, and with these values it can be shown that the the maximum electric field value of 0.6 mV/m corresponds to a wave magnetic field of $\sim$12 mγ.

Taking into account the finite wave normal angle, it can be shown that the maximum electromagnetic wave energy in the high amplitude region is approximately 7 dB below that appropriate to the wave magnetic field given by (4). If this difference in wave energy were due only to ionospheric absorption then this result would argue for a reflection in the E region where the effects of absorption would be minimized.

The theory of *Brinca* [1972] applies to the initial stage of the sideband instability when the sidebands are still very small in amplitude compared to the input wave. In this case only two sidebands are predicted with separation given by (1). No theory presently exists for the later stages of the whistler-mode sideband instability when the sideband amplitude approaches that of the input wave and the instability saturates. Conceivably, the saturation regime could lead to the production of additional sidebands separated from one another in frequency by the value given in (1). Studies of sideband wave generation in electrostatic waves indicate that subsidiary sidebands should be produced in the later stages of the electrostatic sideband instability [*Higuchi*, 1980].

Computer simulation studies of the whistler mode sideband instability have been carried out by *Denavit and Sudan* [1975]. These studies confirm the idea that sideband waves can be generated during interactions between energetic gyroresonant electrons and high amplitude whistler mode waves. Furthermore, this work indicated that in the saturation regime additional sideband waves could also be generated. However, the amplitudes of the upper and lower sidebands produced in the simulation study were generally not similar, in contrast to the observations of February 16. Thus there is only qualitative agreement in a general sense.

Other possible nonlinear mechanisms for producing sidebands include the whistler-mode modulational instability [*Brinca*, 1973; *Karpman et al.*, 1974] and the whistler-mode parametric instability [*Berger and Perkins, 1976*]. However, none of these theories is general enough to predict the presence of multiple sidebands as observed in the February 16, 1983, ISEE 1 satellite data.

5. Summary and Concluding Remarks

The ISEE 1 satellite observations of February 16, 1983 show that coherent VLF signals from ground-based transmitters can achieve average peak electric field amplitudes at $L \sim 3.4$ near the magnetic equatorial plane as high as 0.6 mV/m, a value which corresponds to a wave magnetic field of $\sim$ 12 mγ. According to theory, waves of this amplitude should be quite effective in precipitating energetic electrons from the magnetosphere [*Inan et al.*, 1978], and in trapping energetic electrons to produce large changes in particle energy and pitch angle [*Bell and Inan*, 1981].

Near 1627 UT the peak amplitude of the Omega transmitter signals exceeded by 16 dB the previous maximum measured in the same region and at the same local time. Since the high amplitudes were observed only over a short segment of the orbital path, it appears that the satellite was observing the output of a magnetospheric "hot spot" or VLF wave amplification "cell" in which over a narrow band of frequencies coherent waves were being strongly amplified through the whistler mode instability.

On the basis of the group time delay and amplitude distribution of the Omega signals and the characteristics of whistlers observed in the satellite data we have inferred that the observed high amplitude Omega signals originally propagated along the base of the plasmapause into the southern ionosphere, from which point they had reflected back up to the satellite.

Using a theory of whistler mode sideband generation [*Brinca*, 1972] we have estimated that the Omega signal magnetic field amplitude in the sideband generation region was roughly 16 m γ.

Our results demonstrate that signals from ground based transmitters can achieve high amplitudes in the magnetosphere. Presumably, these high amplitudes result from the coherent whistler mode instability which, from ground based experiments, is known to produce wave growth, sidebands, and VLF emissions [*Helliwell and Katsufrakis*, 1974; *Park*, 1981].

An earlier satellite study of Omega transmitter signals [*Bell et al.*, 1981] and ground based studies of Siple Station transmitter signals [*Carpenter and Miller*, 1976; *Carpenter and Bao*, 1983] found that the coherent whistler mode instabiliy generally was observed usually under conditions of moderate to weak magnetic activity with $Kp < 4$. However the observations reported in the present paper occurred during a time of stronger magnetic activity with $Kp \sim 5$. Thus it is not clear to what extent the high signal amplitudes observed on February 16 are representative of wave amplitudes that could be produced during periods of moderate magnetic disturbance through the coherent whistler mode instability.

Finally, we note that the conditions surrounding the February 16 observations were rather exceptional: the satellite was located close to the magnetic meridian of the transmitter where the input wave amplitude would be highest; the satellite was located in the dawn sector of the magnetosphere where strong wave-particle interactions are known to take place; the magnetic activity was high; and the plasmapause was displaced to a magnetic shell equatorward of the source region. At present we have no other observations in which all the above conditions are satisfied. Thus we cannot judge if these conditions are generally sufficient for the production of high signal amplitudes and associated sideband waves. Satellite studies presently under way should help to answer this question.

6. Appendix

In order to determine the approximate location of the wave amplification region, ray tracing studies in a model magnetosphere were carried out using the Stanford VLF ray tracing program. This program was written by *Walter* [1969] and modified by *Burtis* [1974]; it is similar to that developed by *Kimura* [1966].

The cold plasma density model used is similar to that described in *Inan and Bell* [1977]. In this model it is assumed that the cold plasma density conforms to a diffusive equilib-

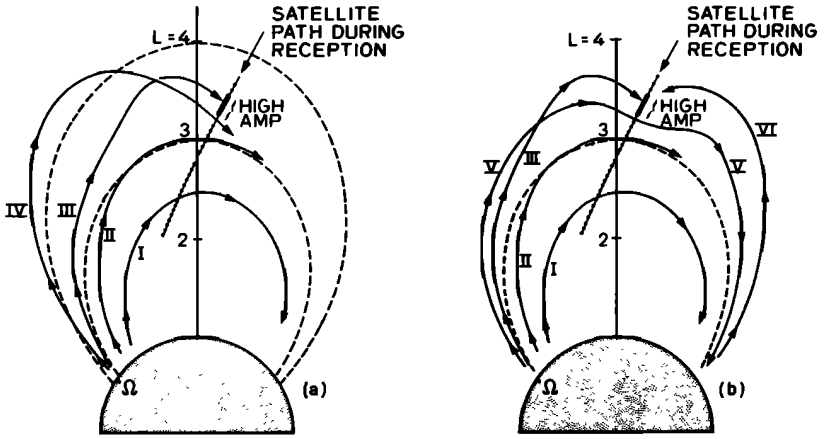

Fig. A1 (*a*). Typical ray paths for 13.1 kHz waves injected into the magnetosphere in the northern hemisphere at 1000 km altitude with vertical wave normal direction. The cold plasma density model used is shown in Figure 10. (*b*) Typical ray paths for 13.1 kHz waves injected into the magnetosphere in the northern hemisphere at 1000 km altitude with vertical wave normal direction. The cold plasma density model includes a 30% density decrease near $L = 3.5$.

rium model [*Angerami and Thomas*, 1964] inside the plasmasphere and to a collisionless model outside the plasmasphere. The cold plasma density variation across the plasmapause has the explicit form:

$$N_{PL} = G(L) + [1 - G(L)]\left[R^a + (1 - R^a)D(r)\right] \quad \text{(A1)}$$

where $G(L) = \text{EXP}(-1/2[(L - L_p)/W]^2)$, $D(r) = \text{EXP}\left[-[(r - r_c)/H_s]^2\right]$, and $R = r_c/r$.

The meaning of the parameters r_c, a, W, H_s, and L_p are given in *Inan and Bell* [1977]. It should be noted that equation (A4) of *Inan and Bell* [1977] contains typographical errors. Equation (A1) above gives the correct variation. In order to fit (A1) to the cold plasma profile shown in Figure 9, the parameter values were chosen: r_c=7370 km, H_s=2000 km, W=0.096, L_p=3.0, and a=3.25. In addition, the temperature of the electrons and ions was chosen to be 1600°K and the ion composition was chosen to be 50% H+ and 50% 0+ at 1000 km altitude. The equatorial cold plasma density at the inner edge of the plasmapause at $L = 3$ was taken to be 1350 cm^{-3}, in keeping with Figure 10.

Ray tracing studies indicated that it was not likely that the high amplitude Omega signals observed on the ISEE 1 satellite had traveled directly to the satellite from their injection points near the transmitter location.

Figure A1*a* shows typical raypaths for waves of 13.1 kHz frequency injected in the northern hemisphere at 1000 km altitude with vertical wave normal direction. The ray paths are plotted only up to the point at which the group time delay equals 900 ms. In our study the injection points were separated by 0.1° in magnetic latitude (λ_m) and ranged from 34° - 65°N. Waves injected with $\lambda_m < 44°$N propagated within the plasmasphere in the nonducted mode along paths similar to that of ray I in Figure A1*a*. The delay time to the satellite along these rays was equal to the measured time delay. None of these rays reached the position of the high amplitude region near $L \sim 3.4$ and $\lambda_m \sim 5°$S. Waves injected with $44°\text{N} \leq \lambda_m \leq 51.5°\text{N}$ were trapped on the inner surface of the plasmapause near $L \sim 3$ and propagated along paths similar to that of ray II of Figure A1*a*. The delay time to the satellite along these rays was equal to the measured time delay. None of these rays reached the high amplitude region. Waves injected with $\lambda_m \geq 52°$N propagated initially in the nonducted mode outside the plasmapause and reached high L shells before returning to the outer surface of the plasmapause near $L \sim 3.3$ where partial ducting along the plasmapause outer boundary took place. This type of ducting is discussed in *Inan and Bell* [1977]. A typical ray with $\lambda_m > 52°$N is ray IV of Figure A1*a*, which was initially traced from $\lambda_m = 53°$N. The segment of ray path shown corresponds to a group time delay of 0.9 s.

Ray III of Figure A1*a* corresponds to a wave injected at 51.6°N. This was the only ray which reached the region of high amplitude, and the group time delay to this region was ~ 0.5 s.

Rays with $51.7°\text{N} \leq \lambda_m \leq 51.9°$N did not reach the region of high amplitude and exhibited a smooth transition between ray type III and IV.

The results illustrated in Figure A1*a* suggests that the satellite position between $L = 3.7$ and $L = 3.5$ may have been inaccessible to vertically injected Omega signals propagating directly from points in the northern hemisphere. Furthermore the single ray to reach the high amplitude region had a group delay of only 0.5 s, significantly less than the observed delay of 0.9 s. However the 0.5-s delay is approximately equal to that observed on the satellite just prior to entry into the high amplitude region.

A much better fit to the data can be obtained by introducing a cold plasma density decrease of 30% near the $L = 3.5$ magnetic shell. The resulting equatorial cold plasma distribution is indicated by the dashed curve in Figure 10. A decrease of this magnitude is consistent with the error in determining the electron density profile at this particular point in space.

The required density decrease is achieved by multiplying the function N_{PL} in (A1) by the function N_D(L), where

$$N_D(L) = 1 \quad L \leq 3.5$$
$$N_D(L) = 0.7 + 0.3\text{EXP}\left[-1/2[10(L - 3.5)]^2\right] \quad \text{(A2)}$$

The half width of this decrease is $\Delta L=0.1$ or approximately 600 km in the magnetic equatorial plane.

Figure A1*b* shows typical ray paths for 13.1 kHz waves injected in the northern hermisphere at 1000 km altitude with vertical wave normal direction. The cold plasma density model used in this study includes the density decrease given in (A2). Rays labeled I and II are identical to those with the same labels in Figure A1*a*. Ray III is substantially identical to ray III of Figure A1*a*, but is perturbed slightly by the density decrease at $L = 3.5$ and arrives at the high amplitude region at a slightly higher L shell but with approximately the same time delay (0.5 s).

Waves injected over the range $51.8° \leq \lambda_m \leq 52.3°$N typically follow the path of ray V. These rays are initially guided by the density decrease at $L = 3.5$ in the same manner as ray II is guided by the density decrease at the plasmapause [*Inan and Bell*, 1977]. The frequency of the guided waves equals one half of the local gyrofrequency near $\lambda_m \sim 13°$ and thereafter the waves are no longer guided by the decrease but propagate toward the outer surface of the plasmapause where they are then guided into the southern ionosphere along the plasmapause outer surface in the manner discussed by *Inan and Bell* [1977]. Waves following ray V do not reach the high amplitude region but cross the magnetic equator at $L = 3.3$ with a time delay of approximately 0.3 s and a wave normal angle in the range 20°–40°. The total propagation time into the southern ionosphere is approximately 0.6 s, and the wave arrives at 1000 km altitude at a latitude of 53° with a wave normal almost perpendicular to the earth's magnetic field. From this point we assume that some of the wave energy is reflected back up towards the high amplitude region either by a specular reflection at the lower boundary of the D region or by strong irregularities in the E region. Ray VI represents the path of such reflected waves which in the case shown have wave normals inclined approximately 25° from the vertical at 1000 km at 53°S latitude. The propagation time of ray VI from 1000 km to the high amplitude region is approximately 0.3 s. Thus the total propagation time along paths V and VI is approximately 0.9 s.

Acknowledgments. We wish to acknowledge the many valuable discussions we have held with our colleagues in the STAR laboratory during the course of this work. The spectrograms and chart used above were prepared by J. Yarbrough. The typescript was prepared by N. Leger. This research was sponsored by the National Aeronautics and Space Administration under contract NAS5-25744.

The Editor thanks I. Kimura and B. Edgar for their assistance in evaluating this paper.

REFERENCES

Ahmed, M., R. C. Sagalyn, P. J. L. Wildman and W. J. Burke, Topside ionospheric trough morphology: occurrence frequency and diurnal, seasonal, and altitude variations, *J. Geophys. Res., 84*, 489, 1979.

Anderson, R. R., and K. Maeda, VLF emissions associated with enhanced magnetospheric electrons, *J. Geophys. Res., 82*, 135, 1977.

Angerami, J. J., Whistler duct properties deduced from VLF observations made with the OGO 3 satellite near the magnetic equator, *J. Geophys. Res., 75*, 6115, 1970.

Angerami, J. J., and J. O. Thomas, Studies of planetary atmospheres, 1, The distribution of electrons and ions in the earth's exosphere, *J. Geophys. Res., 69*, 4537, 1964.

Bell, T. F., and O. Buneman, Plasma instability in the whistler-mode caused by a gyrating electron stream, *Phys. Rev., 133*(5A), A1300, 1964.

Bell, T. F., and R. A. Helliwell, Pulsation phenomena observed in long-duration VLF whistler-mode signals, *J. Geophys. Res., 76*, 8414, 1971.

Bell, T. F., and R. A. Helliwell, The Stanford University VLF wave injection experiment on the ISEE A spacecraft, *IEEE Trans. Geosci. Electron., GE-16*, 248, 1978.

Bell, T. F., and U. S. Inan, Transient nonlinear pitch angle scattering of energetic electrons by coherent VLF wave packets in the magnetosphere, *J. Geophys. Res., 86*, 9047, 1981.

Bell, T. F., U. S. Inan, and R. A. Helliwell, Nonducted coherent VLF waves and associated triggered emissions observed on the ISEE 1 satellite, *J. Geophys. Res., 86*, 4649, 1981.

Bell, T. F., U. S. Inan, I. Kimura, H. Matsumoto, T. Mukai, and K. Hashimoto, EXOS-B/Siple Station VLF wave-particle interaction experiments, 2, Transmitter signals and associated emissions, *J. Geophys. Res., 88*, 295, 1983a.

Bell, T. F., H. G. James, U. S. Inan, and J. P. Katsufrakis, The apparent spectral broadening of VLF transmitter signals during transionospheric propagation, *J. Geophys. Res., 88*, 4813, 1983*b*.

Berger, R. L., and F. W. Perkins, Thresholds of parametric instabilities near the lower-hybrid frequency, Phys. Fluids, 19, 406, 1976.

Brinca, A. L., Whistler sideband growth due to nonlinear wave-particle interaction, *J. Geophys. Res., 77*, 3508, 1972.

Budko, N. I., V. I. Karpman, and O. A. Pokhotelov, Monochromatic circularly polarized VLF and ULF waves in the magnetosphere, *Cosmic Electrodyn., 3*, 147, 1972.

Burtis, W. J., *User's Guide to the Stanford VLF Ray Tracing Program*, Radioscience Laboratory, Stanford Electronics Laboratories, Stanford University, Stanford, Calif., 1974.

Burtis, W. J., and R. A. Helliwell, Magnetospheric chorus: Occurrence patterns and normalized frequency, *Planet. Space Sci., 24*, 1007, 1976.

Carpenter, D. L., Whistlers and VLF noises propagating just outside the plasmapause, *J. Geophys. Res., 83*, 45, 1978.

Carpenter, D. L., and Z. T. Bao, Occurrence properties of ducted whistler-mode signals from the new VLF transmitter at Siple Station, Antarctica, *J. Geophys. Res., 88*, 7051, 1983.

Carpenter, D. L., and C. G. Park, On what ionospheric workers should know about the plasmapause–plasmasphere, *Rev. Geophys. 11*, 133, 1973.

Carpenter, D. L., and T. R. Miller, Ducted magnetospheric propagation of signals from the Siple, Antarctica, VLF transmitter, *J. Geophys. Res., 81*, 2692, 1976.

Cerisier, J. C., A theoretical and experimental study of nonducted VLF waves after propagation through the magnetosphere, *J. Atmos. Terr. Phys., 35*, 77, 1973.

Chang, D. C. D., and R. A. Helliwell, VLF pulse propagation in the magnetosphere, *IEEE Trans. Antennas Propag, AP-28*, 170, 1980.

Chang, D. C. D., R. A. Helliwell, and T. F. Bell, Sideband mutual interactions in the magnetosphere, *J. Geophys. Res., 85*, 1703, 1980.

Das, A. C., A mechanism for VLF emissions, *J. Geophys. Res., 73*, 7457, 1968.

Denevit, J., and R. N. Sudan, Whistler sideband instability, *Phys. Fluids, 18*, 575, 1975.

Dowden, R. L., A. C. McKey, L. E. S. Amon, H. C. Koons, and M. H. Dazey, Linear and nonlinear amplification in the magnetosphere during a 6.6 kHz transmission, *J. Geophys. Res., 83*, 169, 1978.

Dysthe, K. B., Some studies of triggered whistler emissions, *J. Geophys. Res., 76*, 6915, 1971.

Edgar, B. C., The upper and lower frequency cutoffs of magnetospherically reflected whistlers, *J. Geophys. Res., 81*, 205, 1976.

Gurnett, D. A., F. L. Scarf, R. W. Fredericks, and E. J. Smith, The ISEE 1 and ISEE-2 plasma wave investigation, *Geosci. Electron., GE-16*, 225, 1978.

Hashimoto, K., and I. Kimura, A generation mechanism of narrow band hiss emissions above one half the electron cyclotron frequency in the outer magnetosphere, *J. Geophys. Res., 86*, 11,148, 1981.

Helliwell, R. A., Whistlers and Related Ionospheric Phenomena, Stanford University Press, Stanford, Calif., 1965.

Helliwell, R. A., A theory of discrete VLF emissions from the magnetosphere, *J. Geophys. Res., 72*, 4773, 1967.

Helliwell, R. A., Siple station experiments on wave-particle interactions in the magnetosphere, in *Wave Instabilities in Space Plasmas*, edited by P. J. Palmadesso and K. Papaddopoulos, p. 191, D. Reidel, Hingham, Mass., 1979.

Helliwell, R. A., and J. P. Katsufrakis, VLF wave injection into the magnetosphere from Siple Station, Antarctica, *J. Geophys. Res., 79*, 2511, 1974.

Helliwell, R. A., J. P. Katsufrakis, and M. L. Trimpi, Whistler-induced amplitude perturbation in VLF propagation, *J. Geophys. Res., 78*, 4679, 1973.

Helliwell, R. A., S. B. Mende, J. H. Doolittle, W. C. Armstrong, and D. L. Carpenter, Correlations between λ4278 optical emissions and VLF wave events observed at $L \sim 4$ in the Antarctic, *J. Geophys. Res., 85*, 3376, 1980.

Higuchi, Y., Temporal subsideband growth due to secondary distortion of trapped particles, *J. Phys. Soc.* Jpn., 49, 1645, 1980.

Imhof, W. L., J. B. Reagan, H. D. Voss, E. E. Gaines, D. W. Datlowe, J. Mobilia, R. A. Helliwell, U. S. Inan, and J. Katsufrakis, Direct observation of radiation belt electrons precipitation by the controlled injection of VLF signals from a ground-based transmitter, *Geophys. Res. Lett., 10*, 361, 1983*a*.

Imhof, W. L., J. B. Reagan, H. D. Voss, E. E. Gaines, D. W. Datlowe, J. Mobilia, R. A. Helliwell, U. S. Inan and J. Katsufrakis, The modulated precipitation of radiation belt electron by controlled signals from VLF transmitters, *Geophys. Res. Lett., 10*, 615, 1983*b*.

Inan, U. S., and T. F. Bell, The plasmapause as a VLF wave guide, *J. Geophys. Res., 82*, 2819, 1977.

Inan, U. S., T. F. Bell, and R. A. Helliwell, Nonlinear pitch angle scattering of energetic electrons by coherent VLF waves in the magnetosphere, *J. Geophys. Res., 83*, 32,351, 1978.

Karpman, V. I., J. N. Istomin, and D. R. Shklyar, Nonlinear frequency shift and self-modulation of the quasi-monochromatic whistlers in the inhomogeneous plasma (magnetosphere), *Planet. Space Sci., 22*, 859, 1974.

Kimura, I., Effects of ions on whistler mode ray tracing, *Radio Sci., 1*, 269, 1966.

Koons, H. C., B. C. Edgar, R. L. Dowden, C. G. Carrington, and L. E. S. Amon, Multipath Doppler shifts in man-made VLF signals, in *ELF-VLF Radio Wave Propagation*, edited by J. A. Holtet, 311 pp., D. Reidel, Hingham, Mass., 1974.

Koons, H. C., M. H. Dazey, R. L. Dowden, and L. E. S. Amon, A controlled VLF phase-reversal experiment in the magnetosphere, *J. Geophys. Res., 81*, 5536, 1976.

Lashinsky, H. T., T. J. Rosenberg, and D. L. Detrick, Power line radiation: Evidence of van der Pol oscillations, *Geophys. Res. Lett., 7*, 837, 1980.

Likhter, Y. I., O. A. Molchanov, and V. M. Chmyrev, Modulation of spectrum and amplitudes of lower-frequency signal in the magnetosphere, *Sov. Phys. JETP Engl. Transl., 14*, 325, 1971.

McPherson, D. A., H. C. Koons, M. H. Dazey, R. L. Dowden, L. E. S. Amon, and N. R. Thomson, Conjugate magnetospheric transmissions at VLF from Alaska to New Zealand, *J. Geophys. Res., 79*, 1555, 1974.

Newman, C. E., Theoretical study of amplitude pulsations of "key-down" whistler-mode signals in the geomagnetosphere, *J. Geophys. Res., 82*, 105, 1977.

Nunn, D., The sideband instability of electrostatic waves in an inhomogeneous medium, *Planet. Space Sci., 21*, 67, 1973.

Nunn, D., A self-consistent theory of triggered VLF emissions, *Planet. Space Sci., 22*, 349, 1974.

Park, C. G., Generation of whistler-mode sidebands in the magnetosphere, *J. Geophys. Res., 86*, 2286, 1981.

Park, C. G., and D. C. D. Chang, Transmitter simulation of power line radiation effects in the magnetosphere, *Geophys. Res. Lett., 5*, 861, 1978.

Rosenberg, T. J., R. A. Helliwell, and J. P. Katsufrakis, Electron precipitation associated with discrete very low frequency emissions, *J. Geophys. Res., 76*, 8445, 1971.

Walter, F., Nonducted VLF propagation in the magnetosphere, *Tech. Rep. SEL-69-061*, Radiosci. Lab., Stanford Electron. Labs., Stanford Univ., Stanford, Calif., 1969.

Walter, F., and J. J. Angerami, Nonducted mode of VLF propagation between conjugate hemispheres: Observations on OGO's 2 and 4 of the "Walking-Trace" whistler and of Doppler shifts in fixed frequency transmissions, *J. Geophys. Res., 74*, 6352, 1969.

T. F. Bell, STAR Lab, Stanford University, Stanford, CA 94305.

(Received June 18, 1984;
revised October 2, 1984;
accepted October 26, 1984.)